*Physicochem. Probl. Miner. Process., 62(1), 2026, 217880*

http://www.journalssystem.com/ppmp

Physicochemical Problems of Mineral Processing

ISSN 1643-1049


# Optimization of alkali leaching–mixed acid leaching using response surface methodology for removing metallic impurities from quartz

**Haizhang Meng [1,2], Xinyao Wang [1], Shujuan Jin [1], Yuyin Huang [3], Yuxian Feng [2], Xin Gao [2], Yaocong Han [1], Tao Xie [1], Heping Li [1], Lihong Lan [1]**

[1] Guangxi Key Laboratory for Polysaccharide Materials and Modifcations, Guangxi Minzu University, Nanning 530008, China

[2] Institute of New Functional Materials, Guangxi Institute of Industrial Technology, Nanning 530022, China

[3] Guangxi Gangqiao New Building Materials Co., Ltd, Guigang 537116, China

Corresponding author: lanlihong2004@163.com (Lihong Lan)

**Abstract:** In this study, we employed a synergistic process combining alkaline leaching pretreatment with mixed acid leaching to purify quartz sand and efficiently eliminate metallic impurities. First, systematic single-factor optimization was used to determine the optimal alkaline leaching parameters to be a NaOH concentration of 8%, a reaction time of 2 h, and a temperature of 225 ℃. After alkaline leaching, a porous and loose structure was formed on the quartz surface, along with a large number of cracks and pits, which significantly enhanced the mass transfer efficiency of the subsequent acid leaching. Based on this, a ternary mixed acid system ($H_3PO_4$-$H_2SO_4$-$H_2C_2O_4$) was used for pressure leaching. The acid leaching process parameters were optimized using response surface methodology, which determined the optimal conditions to be a temperature of 249 ℃, a solid–liquid ratio of 1:5, and a time of 6 h. After treating the quartz sand with the combined process, the sand's total metallic impurity content was significantly reduced from the initial 523.2 mg/kg to 82.6 mg/kg, which amounts to an overall removal rate of as high as 84.33%. The contents of Al, Ca, Fe, K, Mg, Na, and Ti were 50.4, 8.1, 2.2, 6.9, 2.3, 11.5, and 1.2 mg/kg, respectively.

***Keywords:*** high-purity quartz sand, alkali leaching, mixed acid leaching, response surface methodology

## 1. Introduction

Quartz sand serves as a core foundational material in the industrial production of advanced technologies such as semiconductors, photovoltaics, and high-purity glass, where its purity directly determines end-product performance and reliability. Aluminum (Al), a typical impurity in quartz sand, exists in clay minerals, feldspar inclusions, or as a substitute in the quartz lattice as $Al^{3+}$, where it replaces $Si^{4+}$ (Wei et al., 2023). Owing to its high chemical similarity to silicon, Al ranks among the most challenging impurities to eliminate during purification. The purification of quartz primarily involves two approaches: physical separation and chemical purification. Physical separation utilizes differences in physical properties between quartz sand and mineral impurities to remove most impurities (Deng et al., 2024; He et al., 2024; Yang et al., 2024). This can be accomplished via methods such as flotation and magnetic separation. However, the purity achievable through physical separation is far lower than that attained through chemical purification. Chemical purification exploits differences in chemical properties between quartz and impurities, selectively removing impurities via chemical reactions (Zhu et al., 2020).

In recent years, the alkali leaching–acid leaching synergistic process has gained increasing attention for its high efficiency in impurity removal. Alkali leaching can disrupt the structure of amorphous silica and certain aluminosilicates on the quartz surface, thereby exposing deeper impurities and enhancing the mass transfer efficiency of subsequent acid leaching reactions. Conventional acid leaching systems often involve strong acids such as hydrofluoric acid and nitric acid. Although these processes exhibit high impurity removal efficiency (Shao et al., 2022; Martins et al., 2017), their high corrosiveness and

DOI: 10.37190/ppmp/217880

the challenges associated with treating spent acid solutions pose significant environmental and safety concerns. Research on novel mixed-acid systems remains limited. In light of this, a novel synergistic purification process combining "NaOH alkaline etching—phosphoric/sulfuric/oxalic acid" ternary mixed acid leaching was developed. Alkali corrosion removes surface impurities, while mixed acid systems leverage multi-mechanism synergy; for example, phosphoric acid exhibits selective silicate decomposition with weaker corrosivity than HF (Mifsud et al., 2013), and its phosphate-containing wastewater permits facile flocculation–precipitation removal (Emeish et al., 2013). Sulfuric acid effectively decomposes metal oxide impurities via its strong acidity (Pei et al., 2018; Zhou et al., 2024), and oxalic acid chelates $Fe^{3+}$ into stable complexes for iron removal (Du et al., 2011; Taxiarchou et al., 1997; Zhang et al., 2012). The latter's natural abundance and biodegradability minimize environmental impact.

In this study, we employed a NaOH alkaline etching–ternary acid synergistic leaching purification process. The experimental conditions were optimized using Response Surface Methodology (RSM). We investigated alterations to the quartz surface structure induced by the alkaline leaching treatment and analyzed the impact of these structural changes on the subsequent acid leaching process. Simultaneously, the synergistic impurity removal effect of the mixed phosphoric acid, sulfuric acid, and oxalic acid system was investigated. This research showcases a reliable process optimization scheme for the industrial preparation of high-purity quartz sand.

## 2. Materials and methods

### 2.1. Materials

The quartz sand samples used in this experiment were sourced from Guangxi. They contained particles of varying sizes, and mineral impurities were present on the quartz surfaces. The raw quartz ore was crushed, screened, washed with clean water, and color-sorted to obtain quartz sand of uniform color. The color-sorted quartz samples were placed in standard sieves on a mechanical shaker to separate the quartz sand particles.

The chemical reagents used in the experiments, NaOH, $H_2SO_4$, $H_3PO_4$, and $H_2C_2O_4$ (Sinopharm Chemical Reagent Co., Ltd., China), were of analytical grade, and ultrapure water was employed throughout the experiments. This study also employed the following instruments: a Ceramic Fiber Resistance Furnace, LX0711, Tianjin Laiboterui Instrument Equipment Co., Ltd.; an X-ray Diffractometer (XRD), MiniFlex300, PANalytical B.V.; an Inductively Coupled Plasma Optical Emission Spectrometry (ICP-OES), iCAP, Thermo Fisher Scientific Inc.; a Scanning Electron Microscope (SEM), EVO18, Carl Zeiss AG; and an Electron Probe Micro-Analyzer (EPMA), 8050G, Shimadzu Corporation.

### 2.2. Alkaline leaching

A 6.0 g sample of quartz sand that had been pretreated via calcination–water quenching was weighed and placed into a hydrothermal autoclave liner. A specific volume of NaOH solution was added, and the quartz particles adhering to the liner walls were rinsed using a disposable pipette to ensure a uniform mixture. The sealed autoclave was placed in an oven and heated at designated temperatures to conduct hydrothermal alkaline leaching experiments. The effects of NaOH concentration, leaching time, and leaching temperature on the Al impurity removal rate were then investigated.

The removal rate was determined by quantitative analysis using ICP-OES after digestion:

$$n = \frac{(\alpha_0 - \alpha_1)}{\alpha_0} \times 100\% \quad (1)$$

where $n$ is the removal rate (%), $a_0$ is the elemental content in the original quartz sample (mg/kg), and $a_1$ is the elemental content in the quartz sample after alkali leaching (mg/kg).

### 2.3. Mixed acid leaching

A 2.0 g sample of alkali-leached quartz sand was weighed into a hydrothermal autoclave liner. A mixed acid solution containing 0.4 mol/L $H_3PO_4$, 1.0 mol/L $H_2SO_4$, and 0.044 mol/L $H_2C_2O_4$ was added. Quartz particles adhering to the liner walls were rinsed using a disposable pipette to achieve homogeneous mixing. The sealed autoclave was placed in an oven for hydrothermal acid leaching at

controlled temperatures. The effects of liquid-to-solid ratio, leaching temperature, and leaching time on aluminum removal rate were then evaluated.

The removal rate was calculated similarly using equation (1), where $a_0$ represents the elemental content in the quartz sample after alkali leaching (mg/kg), and $a_1$ represents the elemental content in the quartz sample after acid leaching (mg/kg).

### 2.4. Response surface methodology (RSM)

The Al removal rate was taken as the response value (y). The acid leaching temperature was defined as factor A, with levels of 200, 225, and 250 ℃; the acid leaching time was defined as factor B, with levels of 2, 4, and 6 h; and the liquid–solid ratio was defined as factor C, with levels of 4:1, 6:1, and 8:1. The Box–Behnken design in Design-Expert software was used to optimize the hot-pressed acid leaching process for removing impurities from quartz sand. A three-factor, three-level design was employed, involving 17 experiments in total, including 12 factorial experiments and 5 replications at the center point, as presented in Table 1.

Table 1. Factor–level design table for response surface experiments

| factor | level | | |
|---|---|---|---|
| | -1 | 0 | 1 |
| A/℃ | 200 | 225 | 250 |
| B/h | 2 | 4 | 6 |
| C | 4:1 | 6:1 | 8:1 |

## 3. Results and discussion

### 3.1. Analysis results of the quartz sand raw material

The particle size distribution of the quartz sand is shown in Fig. 1. In this experiment, the particle size of the quartz sand sample was mainly distributed between 140 and 240 μm. An appropriate amount of the quartz sand sample was analyzed using an XRD, as shown in Fig. 2. Comparison of the XRD pattern with standard cards revealed that the characteristic quartz peaks in the experimental raw quartz ore were distinct. In addition, no characteristic peaks of mineral impurities existed, indicating a low mineral impurity content and a high-purity quartz sand sample. The surface morphology of the quartz sand was observed using an SEM, with the results shown in Fig. 3. The quartz surface was smooth with sharp edges, showing no obvious pores or cracks.

Spot scanning of quartz sand specimens was carried out using an EPMA, and mineral composition analysis was performed via WDS. Elements have different characteristic X-ray wavelengths, requiring spectroscopic crystals with different atomic plane spacings to satisfy the conditions for Bragg diffraction. This enables efficient spectroscopy of X-rays characteristic of specific elements and yields wavelength-dispersive spectra. As shown in Fig. 4 the spot scanning analysis results show that the main components are $Al_2O_3$, $SiO_2$, MgO, $K_2O$, and FeO. It is speculated that the impurity minerals are potassium feldspar, muscovite, and hematite, which exist in the form of gangue minerals within the quartz (Duan et al., 2024; Guo et al., 2024; Xia et al., 2024; Zuo et al., 2025). Furthermore, ICP-OES was used to test the metal element content in the quartz sand, with the results shown in Table 2. The main impurities found are Al, K, and Na, among other elements. Of these, the content of Al is the highest, totaling 523.2 mg/kg.

Table 2. Chemical composition of the quartz sand sample/(mg/kg).

| Samples | Impurity elements (mg/kg) | | | | | | | |
|---|---|---|---|---|---|---|---|---|
| | Al | Ca | Fe | K | Mg | Na | Ti | Total |
| Quartz sand specimens | 290.7 | 42.5 | 19.8 | 104.4 | 6.8 | 56.0 | 3.0 | 523.2 |
| After alkaline immersion | 112.5 | 33.0 | 16.1 | 24.4 | 3.9 | 82.6 | 1.1 | 273.6 |
| After mixing and acid leaching | 50.4 | 8.1 | 2.2 | 6.9 | 2.3 | 11.5 | 1.2 | 82.6 |

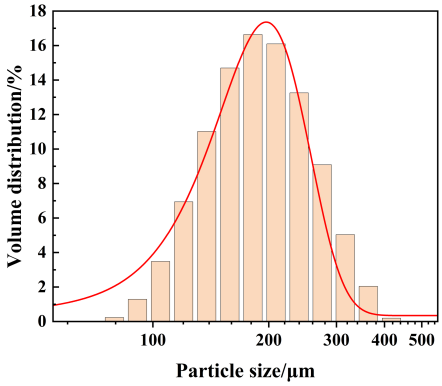


Fig. 1. Particle size analysis of quartz sample

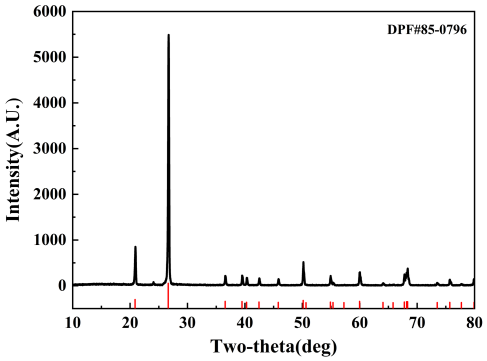


Fig. 2. XRD pattern of quartz sand sample

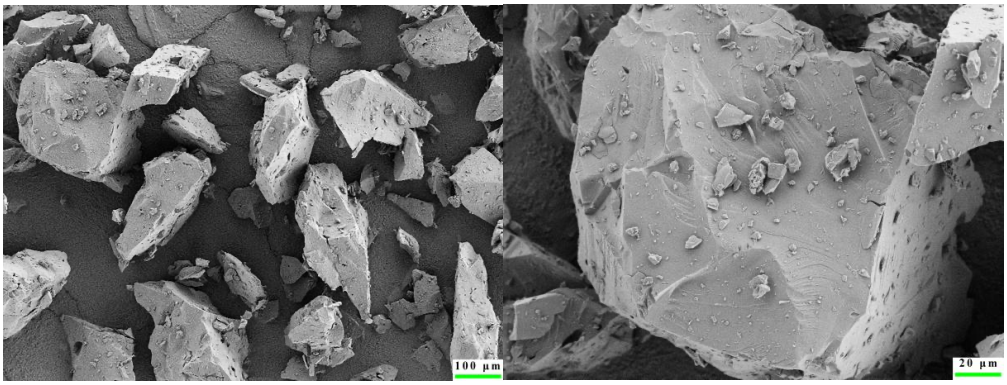


Fig. 3. SEM image of quartz sand sample

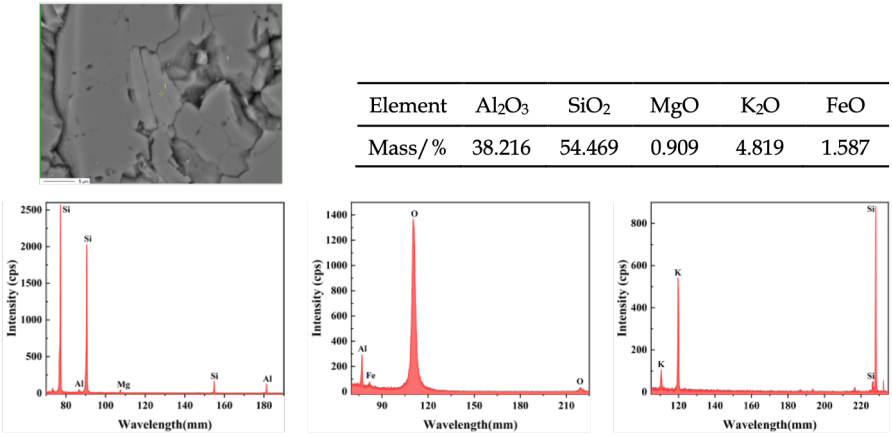

| Element | $Al_2O_3$ | $SiO_2$ | MgO | $K_2O$ | FeO |
|---|---|---|---|---|---|
| Mass/% | 38.216 | 54.469 | 0.909 | 4.819 | 1.587 |

Fig. 4. EPMA spot scanning analysis

### 3.2. Effect of alkali leaching conditions on Al removal rate

#### 3.2.1. Alkali concentration

A total of 5.0 g of the calcined, pretreated quartz sand specimen was weighed into a hydrothermal reactor liner. Then, 2%, 5%, 8%, 11%, and 14% sodium hydroxide solutions were added at a solid–liquid ratio of 1 : 6. Subsequently, hot–pressed alkaline leaching was conducted in a drying oven at 200 ℃ for 2 h. After leaching, the concentration of elemental Al in the quartz was measured via ICP-OES, and the results are presented in Fig. 5.

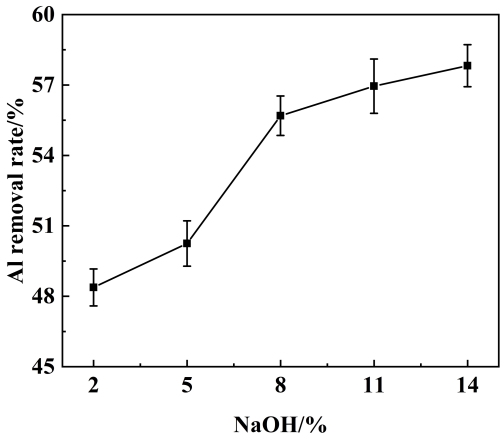


Fig. 5. Effect of NaOH concentration on Al removal rate

As shown in Fig. 5, the Al removal rate generally increased with the rise in NaOH content. Initially, the Al removal rate was 48.37%, but this gradually increased with the NaOH concentration, reaching 55.69% at a NaOH concentration of 8%. Beyond this concentration, further increases in NaOH only resulted in a slight rise in the Al removal rate to a maximum of 57.82% at an 14% NaOH concentration. Therefore, a NaOH concentration of 8% was selected for the experiment.

#### 3.2.2. Alkali leaching time

A total of 5.0 g of calcined pretreated quartz sand specimen was weighed into a hydrothermal reactor liner. Then, an 8% sodium hydroxide solution was added at a solid–liquid ratio of 1 : 6. Hot-pressed alkaline leaching was performed in a drying oven at 200 ℃ for 1, 2, 3, 4, and 5 h. After leaching, the concentration of elemental Al in the quartz was measured via ICP–OES. The results are presented in Fig. 6.

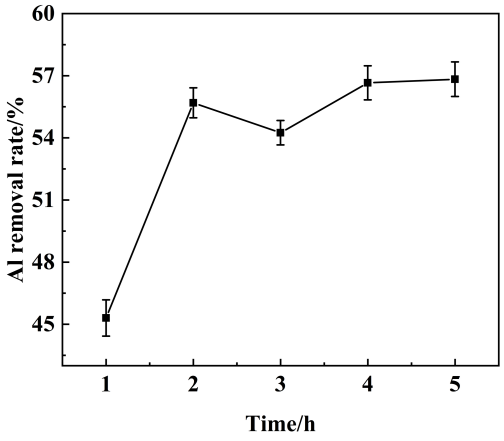


Fig. 6. Effect of alkali leaching time on Al removal rate

As shown in Fig. 6, the Al removal rate tends to increase with the prolongation of alkaline leaching time. At the beginning, the Al removal rate is 45.30%. With the increase of alkaline leaching time, the Al

removal rate rises sharply at first, reaching 55.13% after 2 h of leaching. As the leaching time continues to increase, the Al removal rate increases slowly and gradually approaches equilibrium. Therefore, an alkaline leaching time of 2 h was chosen for the experiment.

### 3.2.3. Alkali leaching temperature

A total of 5.0 g of calcined pretreated quartz sand specimen was weighed into a hydrothermal reactor liner. An 8% sodium hydroxide solution was added at a solid–liquid ratio of 1 : 6. The alkaline leaching temperature was set at 150, 175, 200, 225, and 250 ℃. Hot-pressed alkaline leaching was carried out in a drying oven for 2 h. After leaching, the concentration of elemental Al in the quartz was measured via ICP-OES, and the results are presented in Fig. 7.

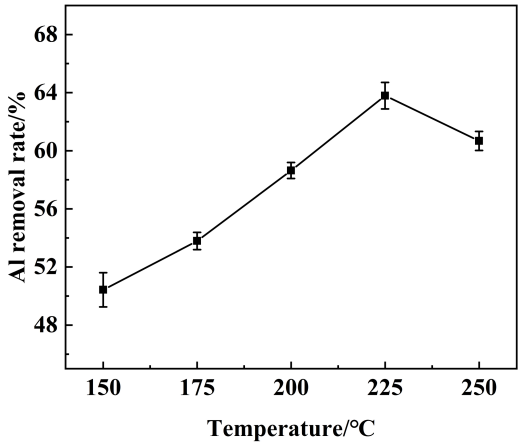


Fig. 7. Effect of alkali leaching temperature on Al removal rate

As shown in Fig. 7, the initial Al removal rate was 50.42%. As the alkaline leaching temperature increased, the Al removal rate rose until it reached 63.78% at 225 ℃. However, further increasing the temperature to 250 ℃ led to a slight decrease in the Al removal rate with some fluctuations that may be attributed to the following factors. In the alkaline leaching system, while NaOH selectively dissolves the active components, the continuous dissolution of quartz—the primary mineral constituent—as temperature increases, leads to a rising concentration of silicate ions in the liquid phase. This favors the formation of hydrated sodium aluminosilicate. When hydrated sodium aluminosilicate precipitates on the surface of quartz particles, it causes reverse migration of dissolved $Al^{3+}$ and results in a surface enrichment effect (Pei et al., 2025). Therefore, an alkaline leaching temperature of 225 ℃ was selected.

Therefore, the optimal conditions for alkaline leaching were determined to be an 8% NaOH concentration, a 2 h alkaline leaching time, and a temperature of 225 ℃ through a one-way test. After alkaline leaching, the elemental content of the quartz sand samples was analyzed using ICP-OES, with the results shown in Table 1. The content of metallic impurities in the quartz sand samples after alkaline leaching was reduced to 273.6 mg/kg, and the total impurity removal rate during alkaline leaching reached 46.81%. Specifically, the Al content decreased to 112.5 mg/kg, while the Na content increased. This is likely because under strong alkaline conditions, the quartz surface may partially dissolve and react with $Na^+$ ions to form silicic acid or hydroxylated surface complexes. Such reactions can cause sodium ions to become embedded in the quartz surface or near-surface area, leading to residual sodium ions that are not completely removed during cleaning, thereby increasing the sodium content.

## 3.3. Effect of alkali leaching on quartz morphology

The morphology of hydrothermally alkali-leached quartz sand was observed using an SEM, as shown in Fig. 8.

Fig. 8 reveals that after hydrothermal alkali leaching, the originally smooth quartz sand surface was damaged, causing it to resemble weathered rock, exhibiting extensive cracks, honeycomb-like pores, and grooves. This is attributed to NaOH corrosion along surface cracks, where the cleavage of Si-O bonds via $SiO_2$ and NaOH reactions caused structural collapse. This process enlarged and deepened

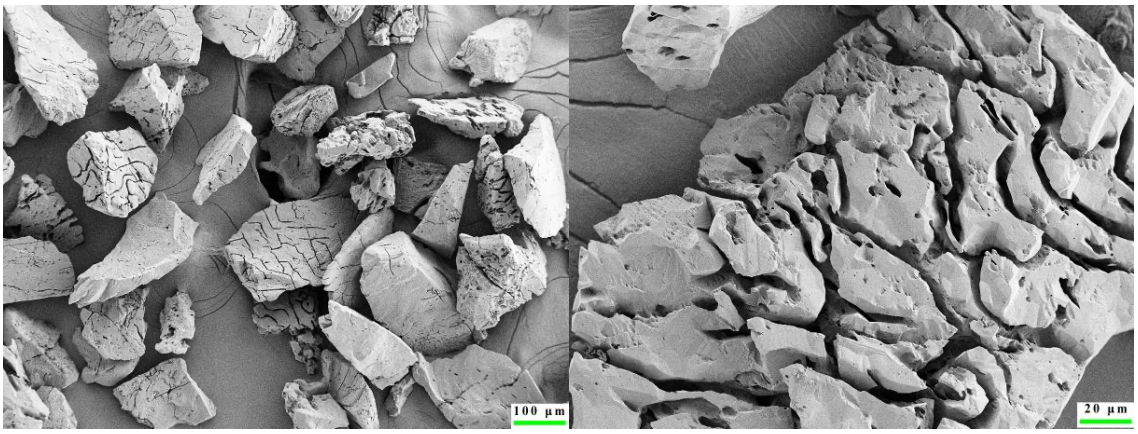


Fig. 8. Surface morphology of quartz sand after alkali leaching

existing fissures, generating substantial corrosion pits. The reaction mechanism is shown in Eq. (2):

$$SiO_2 + 2NaOH = Na_2SiO_3 + H_2O \quad (2)$$

### 3.4. Effect of acid leaching conditions on Al removal rate

#### 3.4.1. Acid leaching solid-liquid ratio

Hydrothermal acid leaching was performed at 200 ℃ for 4 h, using a mixed acid solution containing 0.4 mol/L $H_3PO_4$, 1.0 mol/L $H_2SO_4$, and 0.044 mol/L oxalic acid. Solid–liquid ratios were set at 1:2, 1:4, 1:6, 1:8, and 1:10 to investigate their effect on elemental removal rates. The experimental results are presented in Fig. 9.

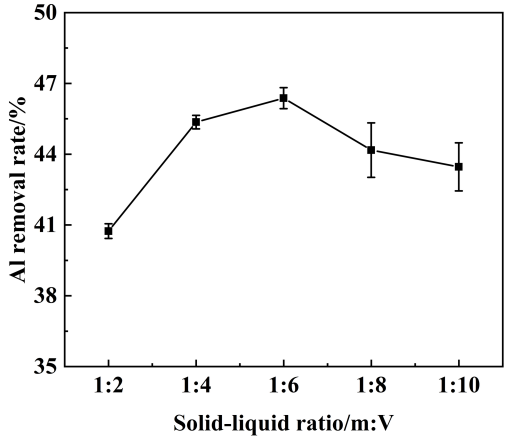


Fig. 9. Effect of solid-liquid ratio on Al removal rate

Fig. 9 demonstrates that the Al removal rate was 40.83% at the initial solid–liquid ratio of 1:2. As the ratio increased to 1:6, the removal rate gradually rose to 46.46%. Beyond this ratio (1:6), the removal rate remained essentially constant. During the experiments, increasing the acid solution volume progressively compressed the vapor space within the fixed-volume reactor liner, which caused a significant pressure buildup in the sealed system. This pressure enhancement intensified chemical interactions between the acid solution and quartz surface impurities, thereby promoting Al removal (Guo et al., 2024). When the acid solution volume exceeded the critical threshold, the concentration gradients of the active components reached dynamic equilibrium. Further addition of acid consequently failed to improve impurity removal efficiency.

#### 3.4.2. Acid leaching temperature

Hydrothermal acid leaching was conducted for 4 h, using a mixed acid solution (0.4 mol/L $H_3PO_4$, 1.0 mol/L $H_2SO_4$, and 0.044 mol/L oxalic acid) at a solid–liquid ratio of 1:6. Leaching temperatures were

set at 150, 175, 200, 225, and 250 ℃ to investigate temperature effects on elemental removal rates. In the interest of operational safety, the temperature was not increased beyond 250 ℃. The results are presented in Fig. 10.

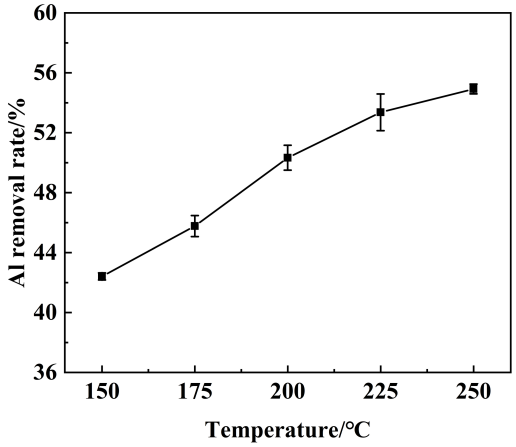


Fig. 10. Effect of acid leaching temperature on Al removal rate

Fig. 10 demonstrates an initial Al removal rate of 42.38% at 150 ℃. As the temperature increased, the removal rate rose rapidly. Above 225°C, the increase became more gradual and stabilized beyond 250 ℃. Consequently, 250 ℃ was selected as the optimal reaction temperature, achieving a 54.83% Al removal rate. Elevated temperatures enhance removal efficiency by increasing the molecular average kinetic energy. This raises the proportion of molecules that overcome the activation energy barrier, resulting in more effective collisions that accelerate reaction kinetics.

### 3.4.3. Acid leaching time

Hydrothermal acid leaching was performed at 250 ℃, using a mixed acid solution (0.4 mol/L $H_3PO_4$, 1.0 mol/L $H_2SO_4$, and 0.044 mol/L oxalic acid) and a solid–liquid ratio of 1:6. Leaching durations were set at 2, 4, 6, 8, and 10 h to investigate time effects on elemental removal rates. The results are presented in Fig. 11.

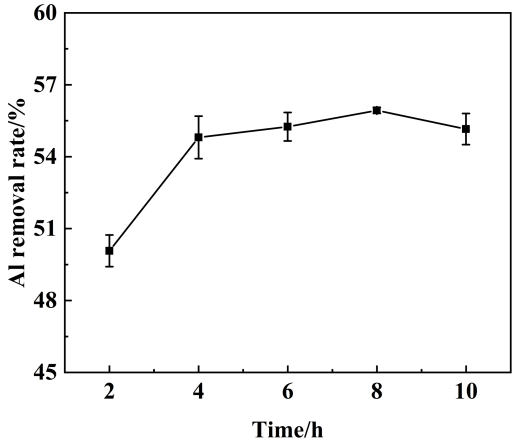


Fig. 11.. Effect of acid leaching time on Al removal rate

Fig. 11 shows an Al removal rate of 50.08% at 2 h. The removal rate increased with leaching time until it reached 56.15% at 4 h. Beyond 4 h, the removal rate stabilized. Initially, rapid reactions between acids and surface impurities accelerated removal efficiency. As these reactions progressed, the depletion of reactive impurities reduced reaction rates, slowing removal efficiency gains. In addition, prolonged leaching after major impurity removal decreased the acid concentration, potentially inducing side reactions such as redeposition (Zang et al., 2016), which could reduce the removal efficiency. Therefore, we selected four hours as the optimal leaching duration.

### 3.5. Analysis of RSM optimization results for mixed acid leaching parameters

The final design parameters obtained from the response surface experiments are shown in Table 3. The results of a variance analysis of the response surface using Design-Expert software are presented in Table 4. The influence of each factor on the response value can be determined through statistical indicators: when the P-value is less than 0.01, the variable has an extremely significant influence; a P-value within the 0.01-0.05 interval is significant; and a P-value greater than 0.05 indicates no significant influence. Specific analysis indicates that the regression model shows high significance (P<0.0001), and F-test results confirm a strong correlation between independent variables and the response value. The lack-of-fit test P-value >0.05 indicates no systematic bias in the model, confirming its rational construction and the accurate reflection of nonlinear relationships in the experimental data (Imron and Titah, 2018; Peng et al., 2020; Shahraki et al., 2018).

The P-values for the single-factor terms A and B are both <0.01, indicating that their main effects reach extremely significant levels. The interaction term BC has a P-value <0.05, indicating significant

Table 3. RSM experimental design and corresponding response values

| SN | A | B | C | Al removal rate/% |
|---|---|---|---|---|
| 1 | -1 | 1 | 0 | 45.87 |
| 2 | -1 | -1 | 0 | 44.9 |
| 3 | 0 | 0 | 0 | 53.16 |
| 4 | -1 | 0 | -1 | 45.27 |
| 5 | 0 | 0 | 0 | 52.07 |
| 6 | 0 | -1 | -1 | 48.07 |
| 7 | 1 | -1 | 0 | 50.18 |
| 8 | 0 | -1 | 1 | 49.06 |
| 9 | 0 | 0 | 0 | 51.44 |
| 10 | 0 | 0 | 0 | 53.87 |
| 11 | 1 | 1 | 0 | 55.15 |
| 12 | 1 | 0 | -1 | 53.88 |
| 13 | 0 | 0 | 0 | 53.44 |
| 14 | 0 | 1 | -1 | 52.01 |
| 15 | 1 | 0 | 1 | 54.01 |
| 16 | -1 | 0 | 1 | 45.51 |
| 17 | 0 | 1 | 1 | 50.69 |

Table 4. ANOVA table for RSM experimental data

| Variance Source | Sum of Square | df | Mean Square | F-value | P-value | |
|---|---|---|---|---|---|---|
| Model | 186.28 | 9 | 20.70 | 29.22 | <0.0001 | Significant |
| A | 125.37 | 1 | 125.37 | 177.02 | <0.0001 | ** |
| B | 16.56 | 1 | 16.56 | 23.38 | 0.0019 | ** |
| C | 0.0002 | 1 | 0.0002 | 0.0003 | 0.9871 | |
| AB | 4.00 | 1 | 4.00 | 5.65 | 0.0491 | * |
| AC | 0.003 | 1 | 0.003 | 0.0043 | 0.9497 | |
| BC | 1.33 | 1 | 1.33 | 1.88 | 0.2123 | |
| $A^2$ | 17.36 | 1 | 17.36 | 24.51 | 0.0017 | ** |
| $B^2$ | 12.76 | 1 | 12.76 | 18.01 | 0.0038 | ** |
| $C^2$ | 5.08 | 1 | 5.08 | 7.17 | 0.0317 | ** |
| Residual | 4.96 | 7 | 0.7082 | | | |
| Lack of Fit | 0.8912 | 3 | 0.2971 | 0.2922 | 0.8300 | Not significant |
| Pure Error | 4.067 | 4 | 1.02 | | | |
| Cor Total | 191.24 | 16 | | | | |

Note: * denotes significance (P<0.05); ** denotes extremely significance (P<0.01)*

main effects. Finally, the quadratic terms $A^2$ and $B^2$ have P-values <0.01, while $C^2$ has a P-value below the 0.05 significance threshold; this confirms significant interaction effects and nonlinear characteristics. This comprehensive evaluation confirms good correlation between this mathematical model and the experiments, enabling effective prediction of process parameter optimization ranges.

Through variance analysis and regression modeling using Design-Expert, the quadratic model was determined to be the most suitable for this experiment. The quadratic polynomial for the response surface regression is given in Eq. (3):

$$R = -153.24725 + 1.54361A + 0.566625B + 3.99775C + 0.02AB - 0.00055AC - 0.144375BC - 0.003249A^2 - 0.435125B^2 - 0.2745C^2 \quad (3)$$

The correlation coefficient and adjusted coefficient for Eq. (3) are R=0.9741 and $R_{Adj}$=0.9407, respectively.

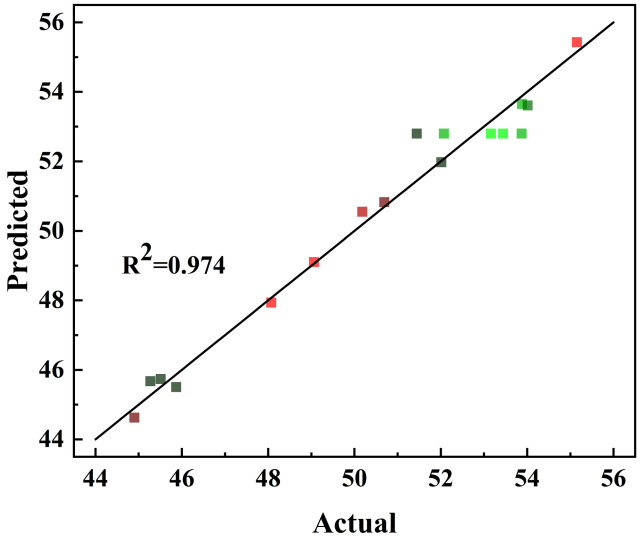


Fig. 12. Correlation between actual and predicted Al removal rates

Fig. 12 shows the relationship between the actual and predicted Al removal rates for this model. The data points are densely distributed along the reference line and are very close to it (y=x). The coefficient of determination, $R^2$=0.974, indicates a high level of agreement between predicted and measured values, confirming the polynomial's fit with the experimental data (Mulay and Rathod, 2022; Yang et al., 2025; Shahraki et al., 2018).

Three-dimensional response surface plots were constructed to visually demonstrate the complex relationships among the acid leaching temperature, acid leaching time, and liquid–solid ratio (Chen et al., 2025; Singh et al., 2025; Sun and Ma, 2025). Figs. 13-15 display 3D response surface plots and their contour plots for pairwise interactions among the three factors. Overall, the surfaces exhibit an inclined unilateral morphology.

As illustrated in Fig. 13 (a), at a constant liquid–solid ratio, the surface gradient changes more significantly with acid leaching temperature adjustments (200-250 ℃) than with time adjustments (2-6 h). In the corresponding contour plot, the temperature contours are denser, while the time contours are sparser. This indicates that minor temperature variations substantially affect Al removal rates, which shows that temperature is more influential than time. It can be observed from Fig. 13 (b) that, at a constant leaching time, the surface gradient varies more steeply with temperature changes (200-250 ℃) than with liquid–solid ratio changes (4-8). The contour plot shows denser temperature contours and less distinct ratio contours, which suggests that temperature has a more pronounced effect than the liquid–solid ratio. The data presented in Fig. 13 (c) demonstrate that, at a constant temperature, the surface gradient changes more gradually with liquid–solid ratio variations (4-8) than with time variations (2-6 h). The contour plot reveals sparser ratio contours and denser time contours, which implies that time has a more significant impact than the liquid–solid ratio.

In conclusion, combined with the F-values in Table 4, the order of influence on Al removal rate is acid leaching temperature > acid leaching time > liquid–solid ratio.

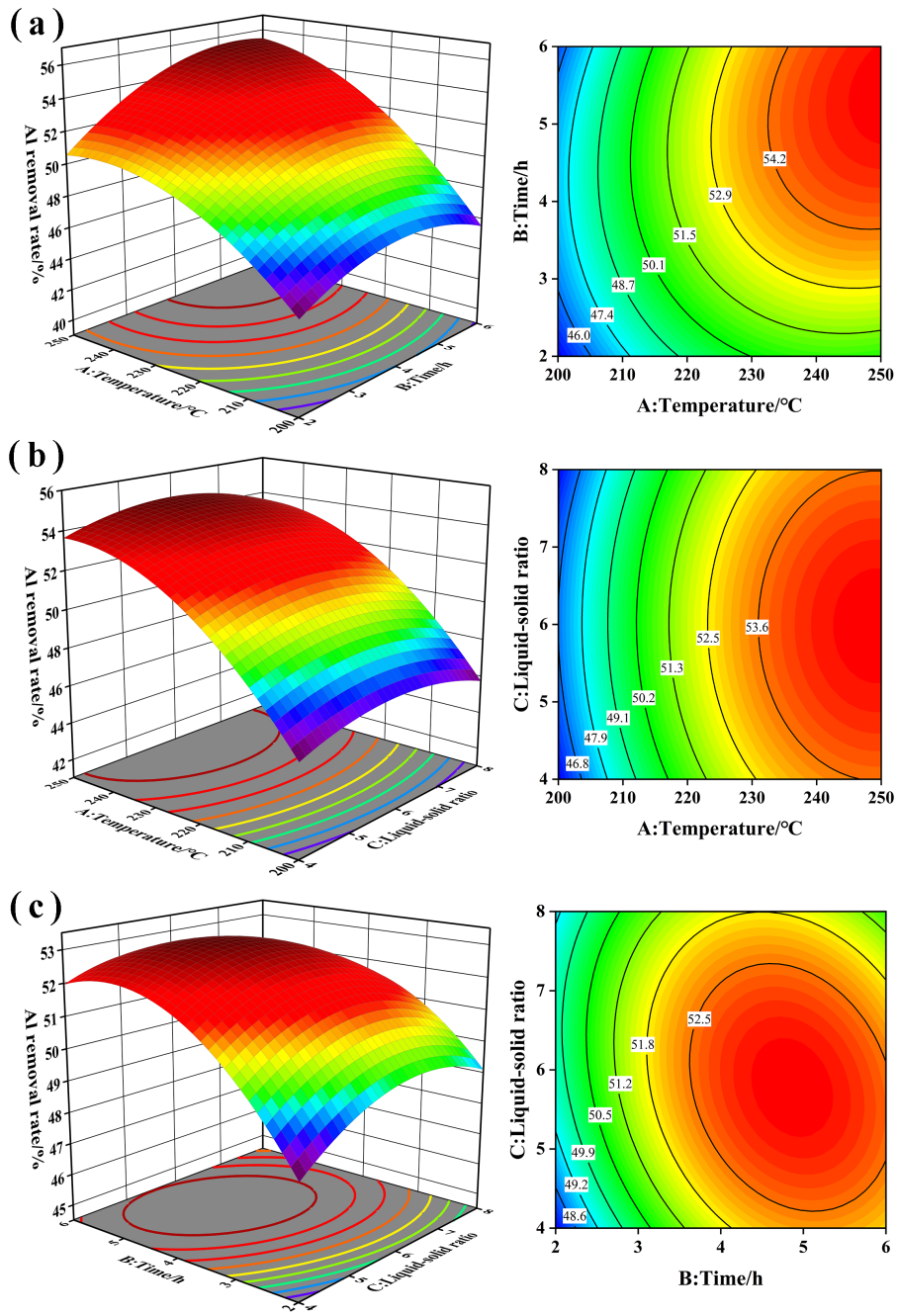


Fig. 13.. 3D response surface and contour plots depicting the interactions between temperature and time (AB), temperature and liquid–solid ratio (AC), and time and liquid–solid ratio (BC)

The RSM mathematical model and its second-order regression equation demonstrate significant reliability, as verified by ANOVA. They accurately describe nonlinear relationships between process parameters and response values, predicting the following optimal conditions: an unchanged mixed acid concentration, a leaching temperature of 249 ℃, a 6 h leaching time, and a 5:1 liquid–solid ratio. The predicted optimal Al removal rate is 55.52%. Validation results are shown in Table 5.

Table 5. Experimental validation results

| No. | Al removal rate / % | Average Al removal rate / % |
|---|---|---|
| 1 | 54.88 | |
| 2 | 55.20 | 54.23 |
| 3 | 52.61 | |

The measured Al removal rate was 2.3% lower than predicted. This comprehensive experimental analysis confirms the tested model's accuracy in predicting Al removal via hydrothermal acid leaching and thereby demonstrates its suitability for quartz sand purification studies.

An ICP-OES analysis of quartz sand leached under optimal conditions was conducted, and the results are shown in Table 2. The residual metallic impurity content after mixed acid leaching was 82.6 mg/kg. This result confirms that the process successfully removes metallic impurities, achieving a purity level characteristic of high-purity quartz. Notably, it attains a purification efficacy on par with traditional hydrofluoric-nitric acid systems, all while striking a balance with environmental sustainability.

## 4. Conclusions

(1) This systematic experimental analysis identified the composition and content of the main metallic impurities in quartz sand raw material. The contents of the main metallic impurities Al, K, Na, Ca, and Fe were 290.7, 104.4, 56.0, 42.5, and 19.8 mg/kg, respectively.

(2) Single-factor experiments determined the optimal alkaline leaching process parameters to be a NaOH concentration of 8%, a reaction time of 2 h, and a temperature of 225 ℃. SEM detection indicated that after alkaline leaching pretreatment, a large number of cracks and corrosion pits were formed on the quartz sand surface, which created favorable conditions for the subsequent acid leaching process.

(3) RSM optimization determined the optimal process parameters for mixed acid pressure leaching to be an acid leaching temperature of 249 ℃, a reaction time of 6 h, and a solid–liquid ratio 1:5. Under these conditions, the total metallic impurity content in the quartz sand was significantly reduced from the initial 523.2 mg/kg to 82.6 mg/kg, thereby achieving an overall removal rate of as high as 84.33%. The contents of Al, Ca, Fe, K, Mg, Na, and Ti were 50.4, 8.1, 2.2, 6.9, 2.3, 11.5, and 1.2 mg/kg, respectively.

(4) Through the aforementioned process, metallic impurities such as Al and Fe in quartz were effectively removed. In practical production applications, methods such as ultrasonic assistance can be employed to enhance the leaching process, reduce the required leaching temperature, thereby lowering costs and improving production safety.

## Acknowledgments

Guangxi Key Research and Development Program (Guike AB23075167); Chongzuo Central Guidance for Local Science and Technology Development Fund (Chongke 2023ZY0502); Guigang City Science Research and Technology Development Plan Project (Guikeji 2203027).

## References

CHEN, K., LU, Q., YONG, X., ZHANG, P., YAN, H., SHI, H., 2025. *Process parameter optimization of SLM AlSi10Mg based on box-behnken design and experimental study on microstructure and mechanical properties.* Mater. Today Commun. 46, 112740.

DENG, J., LUO, D., BAI, J., RONG, K., 2024. *Effect of ultrasonic pretreatment on flotation purification of quartz.* Physicochem. Probl. Miner. Process. 60 (3), 190008.

DU, F., LI, J., LI, X., ZHANG, Z., 2011. *Improvement of iron removal from silica sand using ultrasound-assisted oxalic acid.* Ultrason. Sonochem. 18, 389–393.

DUAN, X., LU, S., FU, Y., ZHANG, J., LIU, T., MA, J., 2024. *Ash removal from inferior coal via ammonium fluoride roasting and simultaneous yield of white carbon black*. Int. J. Min. Sci. Technol. 34, 261–279.

EMEISH, S., ABU-ARABI, M.K., HUDAIB, B.I., 2013. *Removal of phosphate from eshidiya industrial wastewater by sedimentation and enhanced sedimentation.* Desalin. Water Treat. 51, 1629–1633.

GUO, W., LU, H., ZHANG, Z., JIANG, L., WU, H., LIU, D., CHI, R., 2024. *Crystal structure transformation and lattice impurities migration of quartz during chlorine roasting*. Int. J. Min. Sci. Technol. 34, 1465–1474.

HE, Y., REN, Z., ZHU, H., LI, M., ZHENG, R., SONG, Y., CHEN, Z., 2024. *Application of dodecyl amine/dodium petroleum sulfonate mixed collector in quartz-feldspar flotation separation.* Physicochem. Probl. Miner. Process. 60 (1), 185553.

IMRON, M.F., TITAH, H.S., 2018. *Optimization of diesel biodegradation by vibrio alginolyticus using box-behnken design.* Environ. Eng. Res. 23, 374–382.

MARTINS, P.F.F., MORAIS, C.A., LAMEIRAS, F.S., ALBUQUERQUE, R.O., 2017. *Silica and iron recovery from a residue of iron ore flotation.* J. Miner. Mater. Charact. Eng. 5, 153–160.

MIFSUD, C., FUJIOKA, T., FINK, D., 2013. *Extraction and purification of quartz in rock using hot phosphoric acid for in situ cosmogenic exposure dating.* Nucl. Instrum. Methods Phys. Res. B: Beam Interact. Mater. At. 294, 203–207.

MULAY, A., RATHOD, V.K., 2022. *Ultrasound-assisted synthesis of ethyl hexanoate using heterogeneous catalyst: optimization using box-behnken design.* J. Indian Chem. Soc. 99, 100573.

PEI, Z., LIN, M., LIU, Y., LEI, S., 2018. *Dissolution behaviors of trace muscovite during pressure leaching of hydrothermal vein quartz using $H_2SO_4$ and $NH_4Cl$ as leaching agents.* Minerals. 8, 60.

PEI, Z., LEI, S., 2025. *Purifcation Technology and Mechanism of Vein Quartz by Alkaline Leaching.* Non-Metallic Mines. 48, 65–68.

PENG, X., YANG, G., SHI, Y., ZHOU, Y., ZHANG, M., LI, S., 2020. *Box–behnken design based statistical modeling for the extraction and physicochemical properties of pectin from sunflower heads and the comparison with commercial low-methoxyl pectin.* Sci. Rep. 10, 3595.

SHAHRAKI, S., KARAMOOZIAN, M., AZIZI, A., 2018. *Desulfurization of coal by $HNO_3$ leaching: optimization of influential factors using box-behnken design.* J. Min. Environ.

SHAO, H., ZANG, F., JI, M., YU, M., 2022. *Prepare and mechanism of high purity quartz by alkali corrosion and acid leaching process using vein quartz.* Silicon. 14, 12475–12483.

SINGH, N., CHETTY, M., RATHILAL, S., 2025. *Optimising microalgae upscaling for sustainable biomass production using statistical design: a box-behnken, RSM and ANOVA-based approach.* Chem. Eng. J. Adv. 24, 100948.

SUN, K., MA, T., 2025. *Optimization plasma activated water treatment for buckwheat sprouts using a box-behnken design.* Appl. Food Res. 5, 101170.

TAXIARCHOU, M., PANIAS, D., DOUNI, I., PASPALIARIS, I., KONTOPOULOS, A., 1997. *Removal of iron from silica sand by leaching with oxalic acid.* Hydrometallurgy. 46, 215–227.

WEI, Z., LI, Y., LI, P., PAN, L., HU, X., GU, Y., TIAN, Y., 2023. *Migration mechanisms of $Al^{3+}$/$Li^{+}$ lattice impurities during phase transition from a-quartz to β-quartz: an implication for purification of high-purity quartz.* Minerals. 13.

XIA, M., YANG, X., HOU, Z., 2024. *Preparation of High-Purity Quartz Sand by Vein Quartz Purification and Characteristics: A Case Study of Pakistan Vein Quartz.* Minerals 14, 727.

YANG, L., ZHENG, P., CHEN, Z., 2025. *Optimization of the preparation of chitosan nanoparticles loaded with bifendate using the box–behnken design.* Results Chem. 14, 102085.

YANG, S., LUO, X., ZHOU, H., TANG, X., LIU, Z., GUO, J., SHEN, L., 2024. *Effect of sodium hexametaphosphate on the flotation separation of lepidolite and quartz: MD study.* Physicochem. Probl. Miner. Process. 60 (5), 192882.

ZANG, F., LEI, S., ZHONG, L., PEI, Z., YANG, Y., XIONG, K., 2016. *Purification of vein quartz by mixed acid thermal pressure leaching and it's mechanism.* China Mining Magazine. 25, 106–110.

ZHANG, X., WANG, X., DENG, J., MA, Z., YANG, J., CHENG, N., CHEN, J., 2012. *Study on Oxalic Acid Complexation Method of Removing Iron from Quartz.* Bulletin of the Chinese Ceramic Society. 31, 852–855, 860.

ZHOU, H., QI, Z., CHEN, Q., HAN, Y., LI, Y., 2024. *Study on Process Mineralogy and Concentration Experiment of Quartz Ore from Xinjiang Province.* Non-Metallic Mines. 47, 75–77, 81.

ZHU, J., DAI, D.S., LI, L.P., YANG, S., 2020. *An experimental study of removing impurity from a quartz ore by microbial flotation-acid leaching.* Physicochem. Probl. Miner. Process. 57, 18–28.

ZUO, S., GAN, R., WEN, Z., ZHANG, L., JIANG, Z., ZHAO, F., LIU, C., LI, K., XU, Z., 2025. *Effect of acid fracturing fluid modifying coal microstructure stimulated by ultrasonic.* Int. J. Min. Sci. Technol. 35, 275–293.